


Cite this: *RSC Adv.*, 2025, 15, 3172

# Microbial mediated silver nanoparticles enhance the potential of bioactive metabolites in the medicinal plant *Linum usitatissimum*

Minahil Khalid  and Mamoona Noreen \*

Medicinal plants contain phytochemicals that confer therapeutic potentials, allowing plants to perform various biologically significant functions. However, the therapeutic potential of these bioactive metabolites against multidrug-resistant bacteria is limited. Hence, the potential use of rhizospheric bacteria to isolate silver nanoparticles to enhance the potential of bioactive metabolites has been adopted by researchers. Therefore, this research aimed to biogenically produce silver nanoparticles using the rhizospheric soil of *Aloe barbadensis miller* and to evaluate its impact in regulating the potential of bioactive metabolites produced from the medicinal plant *Linum usitatissimum*. The powder extract of *Linum usitatissimum* was macerated under four different environmental conditions including cold maceration, warm maceration, fermented, and unfermented for extraction of metabolites. Macerated extracts were then evaluated for phytochemical detection of bioactive metabolites like alkaloids, steroids, phenols, and saponins. Biogenic AgNPs were primarily confirmed by visible color change from colorless to brown and were further characterized using UV-vis spectroscopy, giving two absorbance peaks at 440 nm and 445 nm. Functional groups attached to biogenic AgNPs were detected by Fourier transform infrared (FTIR) analysis. The crystalline nature of biogenic AgNPs was evaluated by X-ray diffraction (XRD) giving a diffraction peak at angles of around 36°, 46°, 67°, and 77°. The particle size and morphological appearance of biogenic AgNPs were confirmed by Scanning Electron Microscopy (SEM). The total phenolic content of biogenic AgNPs and bioactive metabolites was estimated by the Folin–Ciocalteu (F–C) assay. The antimicrobial efficacy of biogenic AgNPs and bioactive metabolites against MDR bacterial strains was accessed. This research shows that biogenic AgNPs can be used as a strong agent in enhancing the antimicrobial potential of bioactive metabolites against MDR bacteria and they can be investigated for further experimental findings.

Received 29th April 2024  
Accepted 31st December 2024

DOI: 10.1039/d4ra03104k

rsc.li/rsc-advances

## 1. Introduction

Multidrug resistance (MDR) is a major concern all around the globe affecting human health and the social economy. Continuous use of antibiotics leads to the development of drug resistance in several bacterial species.<sup>1</sup> Medicinal plants are considered to be effective sources for treating antimicrobial infections. Many studies have found that the biomedical implications of medicinal plants contribute to the medical field, producing many natural phyto-medical products and bioactive metabolites through a green synthesis approach.<sup>2</sup> One of these medicinal plants belonging to the family Linaceae (*Linum usitatissimum*) is widely used to produce oil, fibers, and biologically active secondary metabolites with antimicrobial properties that inhibit the growth of a wide range of bacteria. The utilization of

flax seeds is increasing, as it lowers the probability of chronic diseases (e.g. cancer) and degenerative disorders (e.g. diabetes).<sup>3</sup>

Flax seeds have a wide range of phytochemical constituents, such as steroids, saponins, flavonoids, tannins, essential oils, fats, and polyphenolic acid, exhibiting Minimum Inhibitory Concentration (MIC) values ranging from 1.0 to 128  $\mu\text{g ml}^{-1}$  against multidrug-resistant bacteria.<sup>4</sup> Phytochemicals of these medicinal plants with biological functions improve human health in the pharmaceutical, food, and agricultural industries.<sup>5,6</sup> Antibiotic resistance is a major concern, developed by 70% of the MDRs bacterial strain that caused around 1.27 million deaths globally.<sup>7</sup> Escalating drug resistance by bacteria has increased the demand to use nanomaterials. Biogenic nanomaterials obtained by the green-synthesis approach have significant therapeutic potential.<sup>8,9</sup> Hence, microbial-mediated synthesis of silver nanoparticles is a current topic of interest and is used as a novel strategy to enhance the potential of bioactive metabolites in combating antimicrobial resistance.

*Aloe vera* (*Aloe barbadensis miller*), which is a xerophytic plant, has potent therapeutic potential against wounds,

Department of Microbiology and Molecular Genetics, The Women University Multan, Mattital Campus, Pakistan. E-mail: minahilasif2324@gmail.com; mamoona.noreen@gmail.com; Tel: +92-333-2696900; +92-334-6992613



widespread infections, inflammation, and multidrug-resistant bacteria.<sup>10</sup> Aloe vera has a wide range of medicinal properties, including antimicrobial resistance, wound healing, gastrointestinal problems, antioxidant, antifungal, antiviral, antitumor, anticancerous, and can also be used against ringworm infections and intestinal amoebiasis. The rhizospheric soil of the plant contains microbial diversity producing a wide range of bioactive compounds used for human health and diseases.<sup>11,12</sup> Microbial-derived nanoparticles from Aloe vera are potent therapeutic agents that have a prophylactic effect against MDR bacteria. The biosynthesis of nanoparticles is eco-friendly and non-hazardous compared to conventional approaches.<sup>1,13</sup> Previously, various metal-based nanoparticles including selenium (Se), gold (Au), titanium (Ti), copper (Cu), and many others have been significantly employed in microbial-mediated synthesis of nanoparticles. Among these, silver nanoparticles have gained the apex focus of researchers due to their reliability and stability in the field of medical science.<sup>14</sup>

Silver nanoparticles have extensive capability for various biomedical applications such as antimicrobial agents, biosensors, drug-delivery articulations, water-purifying agents, and targeted drug delivery *via* drug coating.<sup>15</sup> Biogenic silver nanoparticles are cuboidal, disk, triangular, and octahedron in shape. The toxic nature of biogenic AgNPs depends on the particle size, amount, environment of the medium, and exposure duration to toxic pathogens.<sup>16</sup> Nonetheless, biogenic AgNPs act as potent antifouling, antitumor, anticancerous, and anti-microbial agents. The biogenic synthesis of AgNPs was carried out using leaves, gel-extract, and rhizospheric soil of the Aloe vera plant.<sup>17</sup>

Production of silver-based nanomaterials using a green synthesis approach is spreading worldwide by around 830 tons each year, showing a significant increase in the previous production of silver nanomaterials which was about 340–480 tons per year.<sup>18</sup> In past years, biogenic silver nanoparticles were synthesized using leaves, inner gel extract as well as culture supernatant of *B. flexus*, *S. aureus*, and *B. megaterium*. AgNPs obtained from microbial-mediate synthesis are considered to have more unrivaled medicinal and therapeutic applications.<sup>19–21</sup> In previous studies, research on the enhanced antimicrobial potential of bioactive metabolites of *Linum usitatissimum* using biogenic AgNPs of *Aloe barbadensis miller* against MDR bacteria has not been reported. Hence, in the current research, the synergetic antimicrobial potential of plant-derived bioactive metabolites and microbial-derived silver nanoparticles is used as a novel drug to combat resistance by multidrug-resistant Gram (+) and Gram (–) bacteria. Furthermore, the total phenolic content of bioactive metabolites and biogenic AgNPs were also evaluated. It was predicted that the synthesis of microbial-mediated silver nanoparticles is effective in enhancing the potential of bioactive metabolites and may be used as a cost-effective agent against alternative drugs.

## 2. Materials & methods

Flax seeds from medicinally important plant; *Linum usitatissimum* were collected. For the isolation of bioactive metabolites, the seeds were made free from impurities and ground into a fine

powder using a grinding machine. The powder was stored in an air-tight container until used. The extract was macerated at four different conditions (Cold-maceration, warm-maceration, fermented, and unfermented) for the quantification of bioactive metabolites.

### 2.1. Preparation of bioactive metabolite extracts

**2.1.1. Fermented and unfermented bioactive metabolites of flax seeds.** In the unfermented extraction of bioactive metabolites, 5 g of flaxseed powder was macerated in 120 ml of distilled water. The macerated solution was boiled in the water bath for 10 minutes. The solution was filtered using Whatman filter paper and stored at 4 °C for future experiments. The fermented maceration process of bioactive metabolites was performed by agitating 5 g of flaxseed powder in 120 ml of distilled water. The sample was autoclaved and cooled at room temperature before inoculation. *Lactobacillus* strain was isolated and inoculated in the sample to initiate the process of fermentation which was carried out at 37 °C for 24 hours. After fermentation, the sample was centrifuged at 45 000–50 000 rpm for 18 minutes. The supernatant was discarded and the pellet was stored at 4 °C for future experimental work.

**2.1.2. Cold-macerated and warm-macerated bioactive metabolites of flaxseeds.** 10 g of flaxseed powder was added in 250 ml of the conical flask and diluted with 120 ml of each solvent (methanol, acetone, ethyl acetate, and *n*-hexane) for cold macerated extraction of bioactive metabolites. The flask was incubated at room temperature for 7 days with continuous shaking for 45 minutes after every 24 hours. Using Whatman filter paper, the macerated extracts were filtered and stored at room temperature. The initial and final volume of extract was recorded while drying the filtrate.

In warm macerated extraction of bioactive metabolites, 10 g of flaxseed powder was added in 250 ml of the conical flask and diluted with 120 ml of each solvent (methanol, acetone, ethyl acetate, and *n*-hexane). The flask was placed in a rotary incubator shaker at 67 °C for 24 hours. The extracts were filtered using Whatman filter paper and stored at room temperature for further experimental work. Bioactive metabolites mainly alkaloids, steroids, phenols, and saponins were detected in each macerated extract of flaxseed solution using various biochemical protocols.

**2.1.3. Biochemical analysis of secondary metabolites isolated from different extracts.** Various biochemical tests were performed using the macerated extracts of *Linum usitatissimum* L (flax seeds) to detect the presence of bioactive compounds *i.e.* alkaloids, steroids, phenols, and saponins.<sup>22</sup>

**2.1.3.1 Mayer's test: alkaloids.** 2 ml of each macerated extract was added in separate test tubes. A few drops of mercuric chloride and potassium iodide were added and agitated. The appearance of a cream-colored precipitate indicated the presence of alkaloids.

**2.1.3.2 Test for steroids.** To the macerated sample, 0.1–2 ml of chloroform was added. The solution was then mixed with 0.1 ml H<sub>2</sub>SO<sub>4</sub>. The formation of a red layer indicated the presence of steroids.

**2.1.3.3 Test for phenols.** A test tube was filled with 2 ml of macerated extract each. 2 ml of ferric chloride solution and 2 ml of potassium ferric cyanide were mixed with the macerated sample. The formation of intense colors (blue and green) indicated the presence of steroids.

**2.1.3.4 Test for saponins.** In the macerated extract sample, a few drops of olive oil were added. The appearance of a foamy layer shows the presence of saponin.

## 2.2. Isolation of silver ion tolerant bacteria

The rhizospheric soil of a medicinally significant subtype of the Aloe vera plant (*Aloe barbadensis miller*) was collected in a sterilized polythene bag and transported to the laboratory. Rhizospheric bacteria were isolated by serially diluting ( $10^{-2}$  to  $10^{-3}$ ) the soil samples (7 g) and were prepared by adding 2 ml of silver nitrate solution to 15 ml of each dilution. 3 ml of each dilution sample was inoculated on a free NaCl-Luria-Bertani (LB) agar plate and incubated for 24 hours at 37 °C. For purification, the colonies were subcultured based on their colony morphology on a free-NaCl-LB agar plate.<sup>23</sup>

**2.2.1. Determination of bacterial tolerance to  $\text{Ag}^{+}$ .** 10 ml of free-NaCl Luria-Bertani (LB) broth was prepared by diluting it with various concentrations of silver nitrate (10–13 g/10 ml) to evaluate the bacterial tolerance to silver ions, and inoculating it with an equal concentration of bacterial suspension that is equivalent to 0.5 McFarland bacterium and incubated it at 37 °C for 24 hours. The little volume of content from test tubes containing dilution ( $10^{-2}$  to  $10^{-3}$ ) was inoculated on free NaCl-LB agar plates, and the visible growth on each plate was observed after incubating it at 37 °C for 24 hours.

**2.2.2. Microbial mediated synthesis of AgNPs.** The bacterial strains that were selected based on their colony morphology, were incubated for 48 hours at 37 °C in a shaking incubator after inoculating on 70 ml free-NaCl-LB broth. After the incubation time, the broth culture supernatant was centrifuged at 12 000–15 000 rpm for 15 minutes. For biomass separation, the supernatant from each broth culture tube ( $10^{-2}$  to  $10^{-3}$ ) was passed through a 0.22-micron syringe filter. For the synthesis of biogenic silver nanoparticles, 15 ml of each bacterial supernatant along with 5 ml of silver nitrate solution was added to the sterile test tube. The test tubes containing supernatant and silver nitrate solution were then incubated for 48 hours at 45 °C and the color change in each test tube was observed after 24 hours. The primary confirmation of synthesized biogenic AgNPs was done by the color change from clear to brown in the supernatant. For the confirmation of biogenic AgNPs, the sample was analyzed by UV-vis spectrophotometry in the range of 200–800 nm.

**2.2.3. Characterization of bioactive metabolites and biogenic AgNPs.** Characterization of the bioactive metabolites, biogenic silver nanoparticles, and their combinations was performed using various methods. The formation of biogenic silver nanoparticles was confirmed using a UV-visible spectrophotometer, giving a spectral absorbance peak in the range of 400–600 nm. FTIR spectroscopy was used to identify the functional groups, compounds, and phytochemicals found in bioactive

metabolites, biogenic AgNPs, and their combinations. The IR spectra were recorded in the range of 4000–5000  $\text{cm}^{-1}$ . The pellet of biogenic AgNPs was air-dried into fine powder for structural and crystalline characterization of biogenic AgNPs by Scanning Electron Microscopy (SEM) and X-ray diffraction (XRD).

## 2.3. Total phenolic content of bioactive metabolites and biogenic AgNPs

The total phenolic content of bioactive metabolites and biogenic silver nanoparticles in different combinations ( $0.01 \text{ mg ml}^{-1}$ ) was measured using the Folin–Ciocalteu (F–C) Assay. 50  $\mu\text{l}$  of bioactive metabolites and biogenic silver nanoparticle extract were loaded into wells of a 96-well plate. 0.1 ml (100  $\mu\text{l}$ ) of 10% F–C (Folin–Ciocalteu) reagent and 75  $\mu\text{l}$  of saturated sodium bicarbonate were added into each well and mixed thoroughly by pipetting the wells of a 96-well plate. The 96-well plates were kept at room temperature for about 3 h and absorbance was measured at 760 nm using a microtiter plate reader. The experiment was performed in triplicates using a sample's different dilution concentrations (50–80  $\mu\text{l}$ ). Ascorbic acid was taken as positive control and the calibration curve of test samples was prepared with gallic acid in the range of 0.1–2.5  $\text{mg ml}^{-1}$ .<sup>24</sup>

## 2.4. Synergistic antimicrobial activity of bioactive metabolites and biogenic AgNPs

Antimicrobial activity of bioactive metabolites and biogenic silver nanoparticles was observed against the clinical isolates of



Fig. 1 Sample collection from seeds of medicinal plants *Linum usitatissimum* L.

Table 1 Phytochemical constituents in *Linum usitatissimum* L. (flax seeds)<sup>a</sup>

Flax-seeds (A)	AK1	ST1	PH1	SAP1
FT	—	+	+	—
UFT	Partial +	+	+	—
CM	+	+	+	+
WM	+	Partial +	+	+

<sup>a</sup> (+) Presence of bioactive metabolites, (—) absence of bioactive metabolites. AK = alkaloids, ST = steroids, PH = phenols, SAP = saponins.





*Staphylococcus aureus*, *Klebsiella* sp, *Pseudomonas aeruginosa*, and *Escherichia coli* by using the Agar well diffusion method. Pathogenic bacterial strains were isolated from the skin surfaces of various patients around the amputation, fracture, and IV-branula from the department (Ortho-theter) of Nishtar Hospital Multan and purified on the nutrient agar plate. The culture pathogenic strain was swabbed on a Muller–Hinton agar plate using a sterilized cotton swab. Wells were fabricated on the agar plate using a flame-sterile Pasteur pipette dipped in

70% ethanol. 50  $\mu$ l of each macerated extract of bioactive metabolites and biogenic silver nanoparticles in different dilution ( $10^{-2}$  to  $10^{-3}$ ) combinations were loaded into each corresponding well. The procedure was performed in triplicates using different dilutions of bioactive metabolites and biogenic AgNPs. The cultural plates were then incubated at 35  $^{\circ}$ C for 24 hours. The diameter for each corresponding well was measured in millimeters afterward.

### 3. Results

#### 3.1. Sample collection and isolation of bioactive metabolites

Flax seeds were collected and ground into fine powder using a grinding machine for the isolation of bioactive metabolites (Fig. 1). The powder extract was macerated and incubated at different environmental conditions for the isolation of bioactive metabolites. The presence of alkaloids, steroids, phenols, and saponins was detected in each macerated extract illustrating the following results (Table 1). Color change giving positive and negative results for the formation of bioactive metabolite is shown in Fig. 2.

#### 3.2. Synthesis and characterization of biogenic AgNPs

Silver ion tolerant bacterial sp. were isolated, selected, and purified based on colony morphology. The isolated bacterial strains were estimated for tolerance to  $\text{Ag}^{1+}$  using different concentrations ( $10$ – $13$   $\mu\text{g}/10$  ml) of silver nitrate as shown in Fig. 3. Silver nanoparticles were formed when 5 ml of bacterial supernatant was diluted into 4 ml of silver nitrate and incubated. Color changes from clear to brown show primary confirmation of biogenic silver nanoparticle production for each bacterial strain, and are demonstrated schematically in Fig. 3. The peaks range between 420–480 nm indicating the presence of biogenic silver

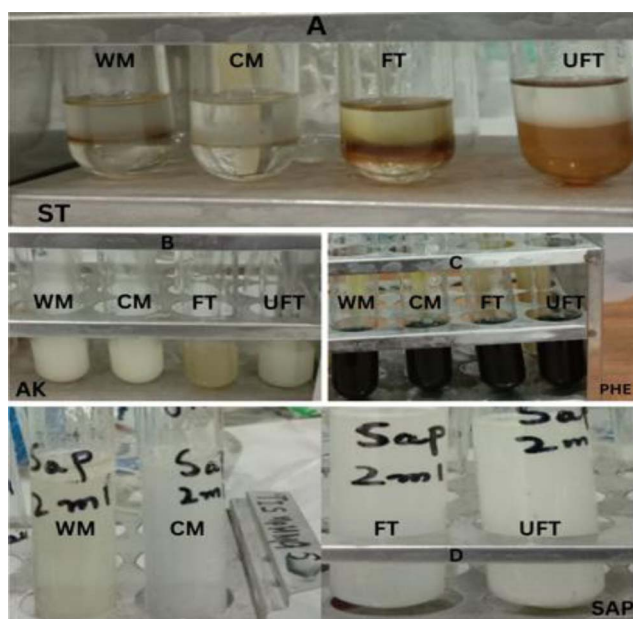


Fig. 2 Detection of bioactive metabolites in aqueous & solvent macerated samples. FT = fermented, UFT = unfermented, CM = cold maceration, WM = warm maceration.

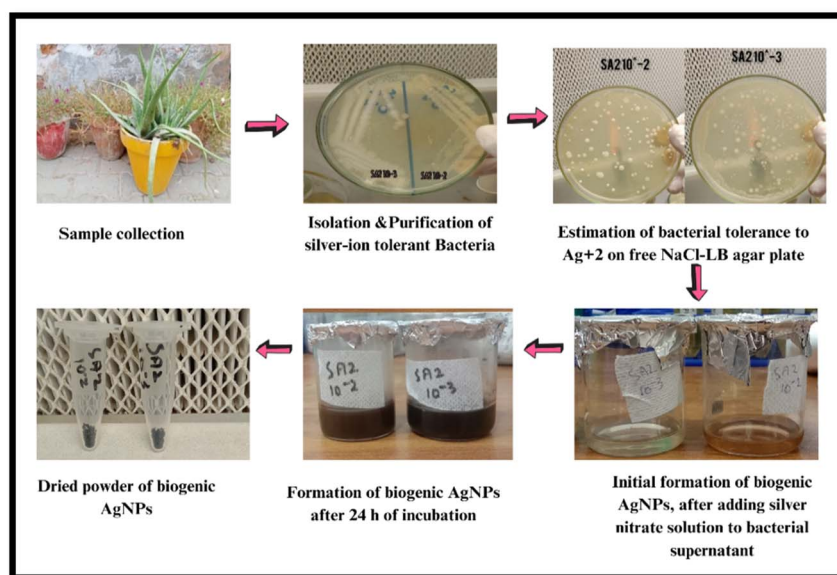


Fig. 3 Graphical representation of the formation of biogenic AgNPs using *Aloe barbadensis miller* rhizopheric soil bacteria. Strain 1:  $\text{SA2 } 10^{-2}$ , strain 2:  $\text{SA2 } 10^{-3}$ .



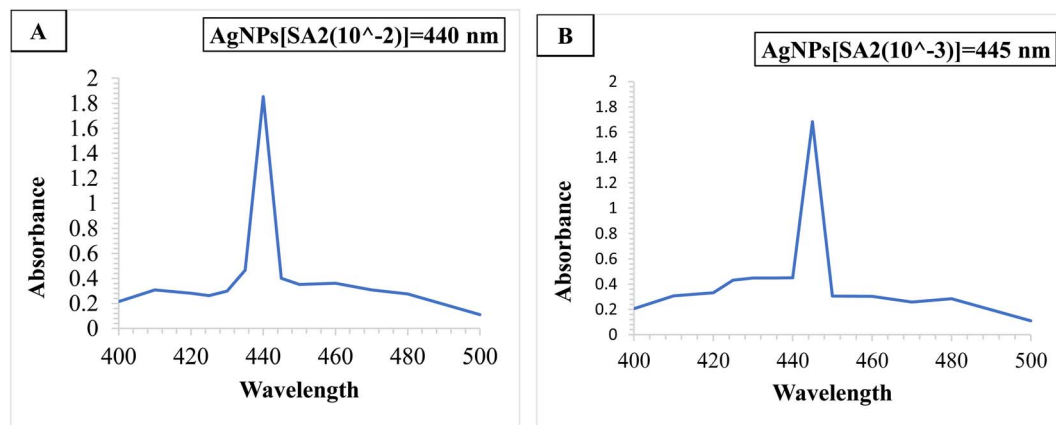


Fig. 4 UV-Visible Spectra for the biogenic synthesis of AgNPs. (A) *Aloe barbadensis miller* AgNPs (SA2  $10^{-2}$ ) showing a sharp peak at 440 nm. (B) *Aloe barbadensis miller* AgNPs (SA2  $10^{-3}$ ) showing a sharp peak at 445 nm. The peaks range between 420–460 nm indicating the presence of AgNPs in the reaction mixture.

nanoparticles in the reaction mixture. Secondary confirmation of biogenic AgNPs for each bacterial strain was performed by UV-vis spectrophotometry where two sharp peaks were observed at 440 and 445 nm (Fig. 4).

FTIR analysis shown in Fig. 5 displays peaks of functional groups O–H, C=C–C, C–H, C–F, CBr for the synergetic combination of (*Linum usitatissimum* L and *Aloe barbadensis miller*) WM+SA2( $10^{-2}$ ) and WM+SA2( $10^{-3}$ ) and comparison of functional groups of the synergetic combinations with the individual samples of biogenic silver nanoparticles and bioactive metabolites (Table 2).

The crystalline nature of biogenic AgNPs was observed by sharp peaks at an angle of  $2\theta$  using X-ray diffraction analysis. The sharp peaks at  $36.24^\circ$ ,  $46.28^\circ$ ,  $67.72^\circ$ , and  $77.25^\circ$  for WM+SA2( $10^{-2}$ ) and peaks at  $36.36^\circ$ ,  $46.48^\circ$ ,  $67.88^\circ$ , and  $77.25^\circ$  for WM+SA2( $10^{-3}$ ) were observed indicating the crystalline nature of biogenic AgNPs as shown in Fig. 6.

SEM analysis shows the particle size of biogenic silver nanoparticles. Particle size and morphological characterization of each biogenic silver nanoparticle were observed under a scanning electron microscope (ZEISS). The synthesized biogenic silver nanoparticles were about 63–64 nm in size and arranged in rocky-crystalline and spherical shape which was estimated with a potential energy of 20 kV and magnification at 10–500 $\times$  as illustrated in Fig. 7.

### 3.3. Estimation of TPC

The total phenolic content for each macerated sample of bioactive metabolites and biogenic AgNPs was estimated using the Folin–Ciocalteu assay (Table 3) grams of gallic acid. This assay is important as it determines the antioxidant potential of bioactive metabolites and biogenic AgNPs, exhibiting the property of neutralizing free radicals affecting the human body. The experiment was performed in triplicates

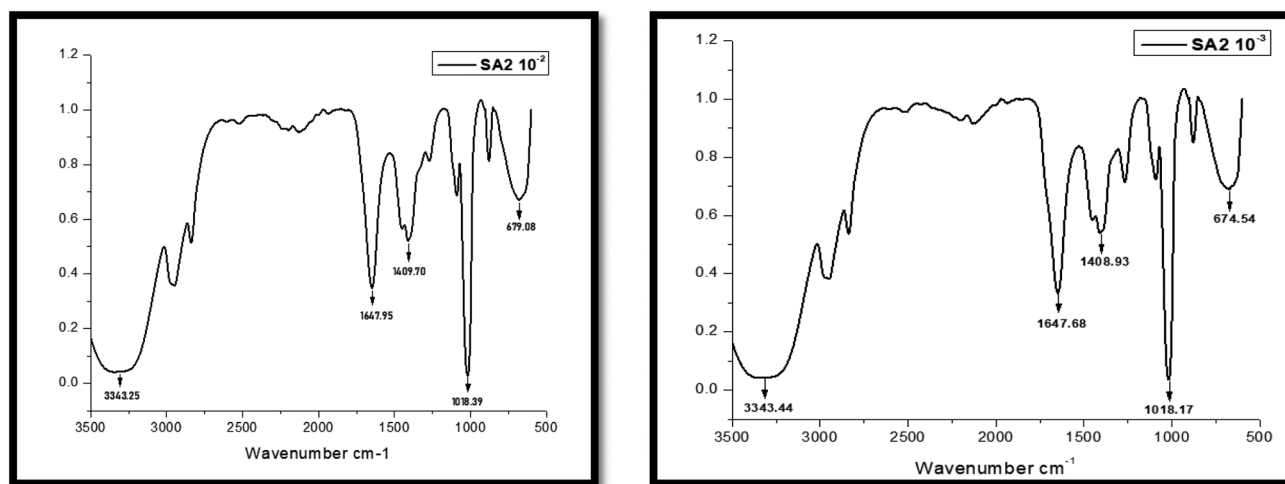


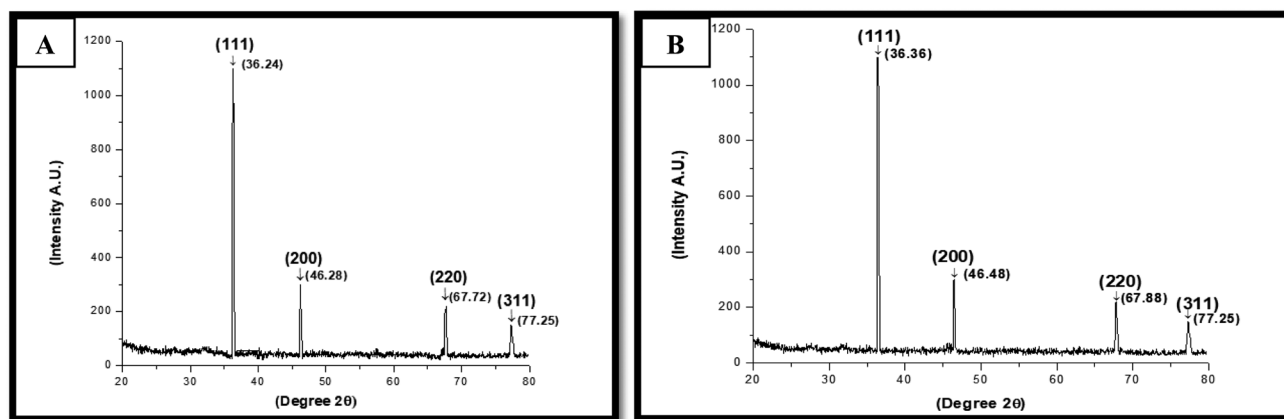
Fig. 5 FTIR analysis of the synergetic combination of warm macerated *Linum usitatissimum* L extract and *Aloe barbadensis miller* AgNPs (SA2  $10^{-2}$ ) and (SA2  $10^{-3}$ )



Table 2 Functional group detection by FTIR analysis for secondary metabolites and AgNPs<sup>a</sup>

S. no.	Sample	Major IR peak positions							
1	UFT	3326.21 O-H group	—	1648.22 C=C-C	1409.05 -CH C=N	1112.49 C-C-C Ether	1016.30 C-F stretch	—	694.58 C-Br, C-S/C-H bend
2	FT	3316.20 O-H group	—	1646.20 C=C-C	—	—	1016.17 C-F stretch	—	675.96 C-Br/C-S/C-H bend
3	WM	3330.86 O-H group	2935.08 -CH methylene	—	1413.95 -CH, C=N	—	1024.33 C-F stretch	880.63 P-O-C stretch	—
4	CM	3342.65 O-H group	2933.75 -CH methylene	1652.96 C=C-C	1413.23 -CH C=N	—	1023.08 C-F stretch	880.19 P-O-C stretch	683.17 C-Br/C-S/C-H bend
5	UFT+SA2(10 <sup>-2</sup> )	3300.35 O-H group	—	1645.38 C=C-C	—	—	1015.61 C-F stretch	—	668.72 C-Br/C-S/C-H bend
6	FT+SA2(10 <sup>-2</sup> )	3280.62 O-H group	—	1643.34 C=C-C	—	—	1015.42 C-F stretch	—	669.68 C-Br/C-S/C-H bend
7	WM+SA2(10 <sup>-2</sup> )	3343.25 O-H group	—	1647.95 C=C-C	1409.70 -CH, C=N	—	1018.39 C-F stretch	—	679.08 C-Br/C-S/C-H bend
8	CM+SA2(10 <sup>-2</sup> )	3328.87 O-H group	—	1642.79 C=C-C	—	—	1016.14 C-F stretch	—	650.15 C-Br/C-S/C-H bend
9	UFT+SA2(10 <sup>-3</sup> )	3285.74 O-H group	—	1645.82 C=C-C	—	—	1015.71 C-F stretch	—	667.52 C-Br/C-S/C-H bend
10	FT+SA2(10 <sup>-3</sup> )	3287.69 O-H group	—	1644.33 C=C-C	—	—	1015.49 C-F stretch	—	665.91 C-Br/C-S/C-H bend
11	WM+SA2(10 <sup>-3</sup> )	3343.44 O-H group	—	1647.68 C=C-C	1408.93 -CH C=N	—	1018.17 C-F stretch	—	674.54 C-Br/C-S/C-H bend
12	CM+SA2(10 <sup>-3</sup> )	3328.19 O-H group	—	1641.48 C=C-C	—	—	1015.94 C-F stretch	—	658.56 C-Br/C-S/C-H bend
13	SA2(10 <sup>-2</sup> )	3325.69 O-H group	—	1636.31 C=C-C	—	—	—	—	631.38 C-Br/C-S/C-H bend
14	SA2(10 <sup>-3</sup> )	3326.85 O-H group	—	1636.23 C=C-C	—	—	—	—	625.02 C-Br/C-S/C-H bend

<sup>a</sup> FT = fermented, UFT = unfermented, CM = cold maceration, WM = warm maceration, UFT+SA2(10<sup>-2</sup>) = unfermented extract and strain one combination, FT+SA2(10<sup>-2</sup>) = fermented extract and strain one combination, CM+SA2(10<sup>-2</sup>) = Cold maceration extract and strain one combination, WM+SA2(10<sup>-2</sup>) = warm maceration extract and strain one combination, UFT+SA2(10<sup>-3</sup>) = unfermented extract and strain two combination, FT+SA2(10<sup>-3</sup>) = fermented extract and strain two combination, CM+SA2(10<sup>-3</sup>) = cold maceration extract and strain two combination, WM+SA2(10<sup>-3</sup>) = warm maceration extract and strain two combination.

Fig. 6 XRD patterns of: (A) *Aloe barbadensis miller* AgNPs (SA2 10<sup>-2</sup>), (B) *Aloe barbadensis miller* AgNPs (SA2 10<sup>-3</sup>)

using different dilution concentrations for each sample. The absorbance was taken at 760 nm. TPC value was measured by taking each sample value as mg of gallic acid equivalence value.

### 3.4. Antimicrobial activity of biogenic AgNPs and bioactive metabolites

**3.4.1. Agar well diffusion method.** The antimicrobial potential of biogenic silver nanoparticles and bioactive

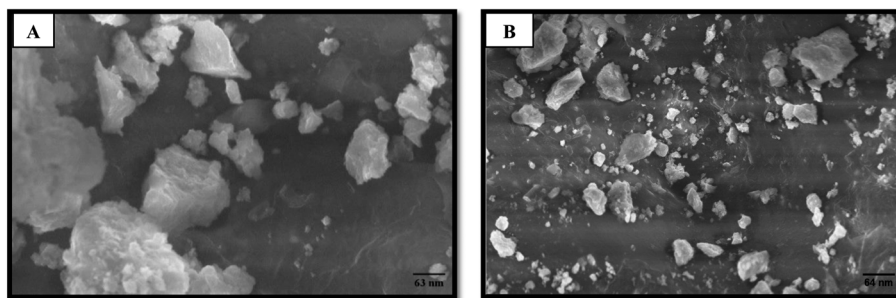


Fig. 7 Characterization of: (A) *Aloe barbadensis miller* AgNPs ( $SA2\ 10^{-2}$ ), (B) *Aloe barbadensis miller* AgNPs ( $SA2\ 10^{-3}$ ) by SEM analysis at different magnifications.

**Table 3** Total phenolic content of bioactive metabolites of *Linum usitatissimum* L and biogenic AgNPs of *Aloe barbadensis miller* and their synergetic combinations<sup>a,f</sup>

No.	Sample	Total phenolic content (mg GA per l <sup>-1</sup> )
1	FT <sup>b</sup>	1.65 ± 0.1 mg l <sup>-1</sup>
2	UFT <sup>b</sup>	0.58 ± 0.3 mg l <sup>-1</sup>
3	CM <sup>b</sup>	1.17 ± 0.1 mg l <sup>-1</sup>
4	WM <sup>b</sup>	1.28 ± 0.1 mg l <sup>-1</sup>
5	SA2(10 <sup>-2</sup> ) <sup>c</sup>	1.40 ± 0.1 mg l <sup>-1</sup>
6	SA2(10 <sup>-3</sup> ) <sup>c</sup>	1.53 ± 0.3 mg l <sup>-1</sup>
7	FT+SA2(10 <sup>-3</sup> ) <sup>d</sup>	1.49 ± 0.1 mg l <sup>-1</sup>
8	UFT+SA2(10 <sup>-3</sup> ) <sup>d</sup>	4.30 ± 0.3 mg l <sup>-1</sup>
9	CM+SA2(10 <sup>-3</sup> ) <sup>d</sup>	1.49 ± 0.1 mg l <sup>-1</sup>
10	WM+SA2(10 <sup>-3</sup> ) <sup>d</sup>	4.98 ± 0.3 mg l <sup>-1</sup>
11	FT+SA2(10 <sup>-2</sup> ) <sup>e</sup>	1.57 ± 0.1 mg l <sup>-1</sup>
12	UFT+SA2(10 <sup>-2</sup> ) <sup>e</sup>	1.24 ± 0.2 mg l <sup>-1</sup>
13	CM+SA2(10 <sup>-2</sup> ) <sup>e</sup>	4.56 ± 0.2 mg l <sup>-1</sup>
14	WM+SA2(10 <sup>-2</sup> ) <sup>e</sup>	1.59 ± 0.1 mg l <sup>-1</sup>

<sup>a</sup> Sample values are expressed in terms of standard deviation,  $n = 3$ .

<sup>b</sup> mg of gallic acid per l of the macerated extracts. <sup>c</sup> mg of gallic acid per l of the biogenic AgNPs. <sup>d</sup> mg of gallic acid per l of the macerated extracts and biogenic AgNPs SA2(10<sup>-3</sup>) mixture. <sup>e</sup> mg of gallic acid per l of the macerated extracts and biogenic AgNPs SA2(10<sup>-2</sup>) mixture.

<sup>f</sup> FT = fermented, UFT = unfermented, CM = cold maceration, WM = warm maceration, UFT+SA2(10<sup>-2</sup>) = unfermented extract and strain one combination, FT+SA2(10<sup>-2</sup>) = fermented extract and strain one combination, CM+SA2(10<sup>-2</sup>) = cold maceration extract and strain one combination, WM+SA2(10<sup>-2</sup>) = warm maceration extract and strain one combination, UFT+SA2(10<sup>-3</sup>) = unfermented extract and strain two combination, FT+SA2(10<sup>-3</sup>) = fermented extract and strain two combination, CM+SA2(10<sup>-3</sup>) = cold maceration extract and strain two combination, WM+SA2(10<sup>-3</sup>) = warm maceration extract and strain two combination.

metabolites was recorded against each pathogenic bacterial strain on the MHA agar plate (Fig. 8). The procedure was performed in triplicates using different concentrations of biogenic AgNPs (20 and 25 mg) and bioactive metabolites (50 and 60 µl) of flaxseeds as shown in Tables 4 and 5. The diameter of the inhibition zone for each corresponding flaxseed well (Fig. 9A and B) was measured after the incubation time.

## 4. Discussion

Biogenically synthesized silver nanoparticles were widely used as herbal medicine in treating a wide range of MDR infections.

Silver nanoparticles were successfully synthesized using a microbial-mediate-synthesis approach by isolating silver ion tolerant bacteria from *Aloe barbadensis Miller* and regulating the antimicrobial potential of bioactive metabolites of *Linum usitatissimum* towards multidrug-resistant bacteria. The formation of biogenic AgNPs was primarily confirmed by visible color change from colorless to brown after adding silver nitrate solution to the broth. Previous studies reported visible changes in the color of silver nanoparticles from clear to dark brown giving initial confirmation of biogenic AgNPs.<sup>25,26</sup>

Experimental findings from the UV-visible absorption spectrum showed the appearance of 2 strong peaks at around 440 nm and 445 nm for *Aloe barbadensis miller* AgNPs. In previous studies, silver nanoparticles showed the strongest peaks at 417 nm, 420 nm, 425 nm, and 470 nm.<sup>27–29</sup> The exact numerical value varies from procedure to procedure but the primary Surface Plasmon Resonance (SPR) range of biogenic silver nanoparticles lies between 420–480 nm and 400–470 nm.<sup>30,31</sup> The experimental results show that the SPR of biogenic AgNPs is affected by the particle size, chemical compounds, and environmental factors of the surrounding medium.<sup>32</sup>

Fourier transformed infrared spectroscopy technique was used to identify the functional groups in each sample and combination. Depending on the fingerprint region of the peaks, position, functional groups, peaks, and intensities for all the extracts, AgNPs and their combinations may be identified. The spectrum of the synergetic potential of combination (*Linum usitatissimum* L and *Aloe barbadensis miller*) WM+SA2(10<sup>-2</sup>) and WM+SA2(10<sup>-3</sup>) showed peaks at 3343.25 cm<sup>-1</sup>, 3343.44 cm<sup>-1</sup>, 1647.95 cm<sup>-1</sup>, 1647.68 cm<sup>-1</sup>, 1409.70 cm<sup>-1</sup>, 1408.93 cm<sup>-1</sup>, 1018.39 cm<sup>-1</sup>, 1018.17 cm<sup>-1</sup>, 679.08 cm<sup>-1</sup>, 674.54 cm<sup>-1</sup> corresponding to functional groups O–H, C=C–C, C–H, C–F, C–Br. FTIR shows an absorbance peak from 3660 cm<sup>-1</sup> to 3200 cm<sup>-1</sup> for –OH stretch, 1650 to 1615 cm<sup>-1</sup> for C = O stretch, 1400 cm<sup>-1</sup> for phenol, 1408 cm<sup>-1</sup> for alkane 1035 cm<sup>-1</sup> to 1014 cm<sup>-1</sup> for C–F stretch and 680 cm<sup>-1</sup> to 650 cm<sup>-1</sup> for C–Br, C–S stretch, and C–H bend. In the previous studies, FTIR shows absorption peaks at 3650 cm<sup>-1</sup> for –OH stretch, 3650 cm<sup>-1</sup> for C–H stretch, 1408 cm<sup>-1</sup> for phenol, and 1246 cm<sup>-1</sup>, 1159 cm<sup>-1</sup> for secondary alcohols.<sup>33,34</sup> These experimental findings were compared with the previous results which showed the presence of the same





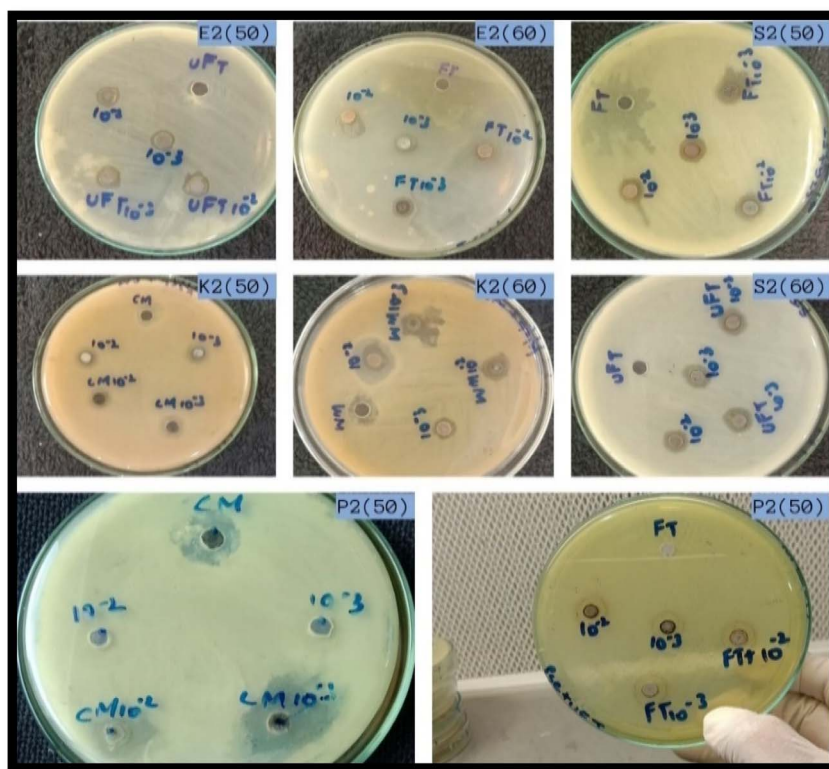


Fig. 8 MH-Agar plate showing the strong antimicrobial effect of *Linum usitatissimum* L extract and *Aloe barbadensis miller* AgNPs (SA2  $10^{-2}$  to  $10^{-3}$ ) strain at a concentration of 50–60  $\mu$ l.

alcohol, amines, aliphatic amines, aldehydes, aromatics, phenols, alkanes, alkenes, alkynes, nitro compounds alkyl halides, primary and secondary amines.<sup>35,36</sup>

X-ray diffraction (XRD) peaks indicate the crystalline nature of biogenic AgNPs. Four sharp peaks at  $36.24^\circ$ ,  $46.28^\circ$ ,  $67.72^\circ$ ,

and  $77.25^\circ$  for WM+SA2( $10^{-2}$ ) and peaks at  $36.36^\circ$ ,  $46.48^\circ$ ,  $67.88^\circ$ , and  $77.25^\circ$  for WM+SA2( $10^{-3}$ ) designated to the plane of (111), (200), (200) and (311) were observed indicating crystalline nature of biogenic AgNPs. In previous studies, diffraction peaks

Table 4 Antimicrobial activity of *Linum usitatissimum* L extract and *Aloe barbadensis miller* AgNPs(SA2) strains at a concentration of 50  $\mu$ l<sup>a</sup>

No.	Sample	<i>E. coli</i>	<i>Klebsiella pneumoniae</i>	<i>Staphylococcus aureus</i>	<i>Pseudomonas aeruginosa</i>
1	FT	—	—	—	—
2	SA2( $10^{-2}$ )	11 mm	10 mm	11 mm	9 mm
3	SA2( $10^{-3}$ )	10 mm	9 mm	11 mm	8 mm
4	FT+SA2( $10^{-2}$ )	8 mm	4 mm	13 mm	13 mm
5	FT+SA2( $10^{-3}$ )	8 mm	11 mm	13 mm	12 mm
6	UFT	6 mm	10 mm	8 mm	—
7	UFT+SA2( $10^{-2}$ )	9 mm	11 mm	13 mm	9 mm
8	UFT+SA2( $10^{-3}$ )	14 mm	22 mm	15 mm	13 mm
9	CM	—	13 mm	—	—
10	CM+SA2( $10^{-2}$ )	10 mm	13 mm	10 mm	10 mm
11	CM+SA2( $10^{-3}$ )	10 mm	10 mm	10 mm	10 mm
12	WM	13 mm	15 mm	15 mm	12 mm
13	WM+SA2( $10^{-2}$ )	13 mm	16 mm	11 mm	13 mm
14	WM+SA2( $10^{-3}$ )	14 mm	22 mm	15 mm	13 mm

<sup>a</sup> FT = fermented, UFT = unfermented, CM = cold maceration, WM = warm maceration, UFT+SA2( $10^{-2}$ ) = unfermented extract and strain one combination, FT+SA2( $10^{-2}$ ) = fermented extract and strain one combination, CM+SA2( $10^{-2}$ ) = cold maceration extract and strain one combination, WM+SA2( $10^{-2}$ ) = warm maceration extract and strain one combination, UFT+SA2( $10^{-3}$ ) = unfermented extract and strain two combination, FT+SA2( $10^{-3}$ ) = fermented extract and strain two combination, CM+SA2( $10^{-3}$ ) = cold maceration extract and strain two combination, WM+SA2( $10^{-3}$ ) = warm maceration extract and strain two combination.





**Table 5** Antimicrobial activity of *Linum usitatissimum* L extract and *Aloe barbadensis miller* AgNPs(SA2) strain at a concentration of 60  $\mu\text{l}$ <sup>a</sup>

No.	Sample	<i>E. coli</i>	<i>Klebsiella pneumoniae</i>	<i>Staphylococcus aureus</i>	<i>Pseudomonas aeruginosa</i>
1	FT	—	12 mm	11 mm	—
2	SA2( $10^{-2}$ )	11 mm	12 mm	12 mm	11 mm
3	SA2( $10^{-3}$ )	8 mm	8 mm	11 mm	12 mm
4	FT+SA2( $10^{-2}$ )	12 mm	13 mm	13 mm	13 mm
5	FT+SA2( $10^{-3}$ )	10 mm	13 mm	15 mm	13 mm
6	UFT	8 mm	4 mm	9 mm	7 mm
7	UFT+SA2( $10^{-2}$ )	12 mm	11 mm	14 mm	12 mm
8	UFT+SA2( $10^{-3}$ )	12 mm	13 mm	14 mm	13 mm
9	CM	9 mm	12 mm	10 mm	6 mm
10	CM+SA2( $10^{-2}$ )	11 mm	13 mm	12 mm	13 mm
11	CM+SA2( $10^{-3}$ )	12 mm	14 mm	12 mm	13 mm
12	WM	11 mm	13 mm	11 mm	—
13	WM+SA2( $10^{-2}$ )	13 mm	11 mm	12 mm	13 mm
14	WM+SA2( $10^{-3}$ )	13 mm	18 mm	17 mm	22 mm

<sup>a</sup> FT = fermented, UFT = unfermented, CM = cold maceration, WM = warm maceration, UFT+SA2( $10^{-2}$ ) = unfermented extract and strain one combination, FT+SA2( $10^{-2}$ ) = fermented extract and strain one combination, CM+SA2( $10^{-2}$ ) = cold maceration extract and strain one combination, WM+SA2( $10^{-2}$ ) = warm maceration extract and strain one combination, UFT+SA2( $10^{-3}$ ) = unfermented extract and strain two combination, FT+SA2( $10^{-3}$ ) = fermented extract and strain two combination, CM+SA2( $10^{-3}$ ) = cold maceration extract and strain two combination, WM+SA2( $10^{-3}$ ) = warm maceration extract and strain two combination.

were detected in the range of 36°, 46°, 67°, and 77° representing crystalline properties of biogenic AgNPs.<sup>27–31,37</sup>

Scanning Electron Microscopy (SEM) images predicted that the produced biogenic AgNPs were about 20–80 nm in size, rocky-crystalline, and spherical. The particle size of *Aloe barbadensis miller* AgNPs was about 63 nm and 64 nm. In previous studies, particle size distribution was reported in the range of 5–50 nm, 20–75 nm, and 65–80 nm and was spherical and octahedrons respectively.<sup>34–38</sup> SEM analysis is crucial for biogenic AgNPs because it provides diameter of particles of different size.

Folin–Ciocalteu assay was used to determine the amount of phenolic compound in each macerated sample of bioactive metabolites and biogenic AgNPs that are crucial in maintaining the stability of bioactive metabolites and biogenic AgNPs. The experiment has shown that a synergetic combination of

bioactive metabolites and biogenic AgNPs enhances the anti-oxidant activities and properties of phenolic compounds. Phenolic compound concentration was estimated in each macerated sample and bioactive metabolites individually and in synergetic combinations showing maximum TPC in synergetic potential of combination (*Linum usitatissimum* L and *Aloe barbadensis miller*) WM+SA2( $10^{-3}$ )  $4.98 \pm 0.3 \text{ mg l}^{-1}$ . Previously reported total phenolic content of AgNPs and bioactive metabolites was about  $3.45 \pm 0.1 \text{ mg l}^{-1}$  and  $2.19 \pm 0.1 \text{ mg l}^{-1}$ .<sup>39,40</sup>

Bacterial pathogenic strains (*Staphylococcus aureus*, *Klebsiella* sp, *Pseudomonas aeruginosa*, and *Escherichia coli*) isolated from various skin samples were resistant to some bioactive metabolites. The synergetic antimicrobial potential of bioactive metabolites and biogenic AgNPs shows significant antimicrobial activity against MDR bacteria and proves to be

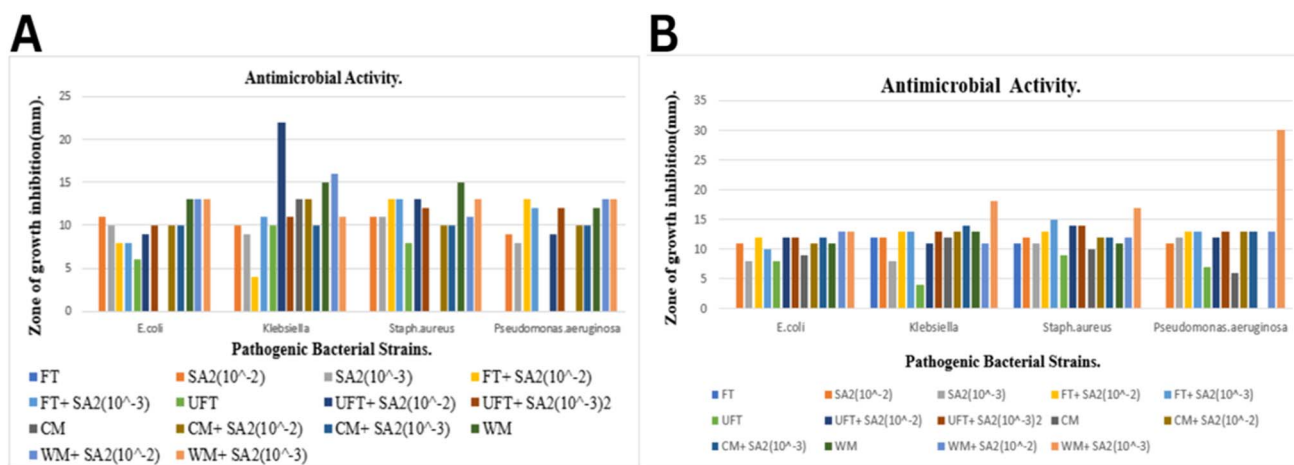


**Fig. 9** (A) Measurement of the zone of inhibition of *Linum usitatissimum* L extract and *Aloe barbadensis miller* AgNPs (SA2  $10^{-2}$  to  $10^{-3}$ ) at a concentration of 50  $\mu\text{l}$ . (B) Measurement of the zone of inhibition of *Linum usitatissimum* L extract and *Aloe barbadensis miller* (SA2  $10^{-2}$  to  $10^{-3}$ ) at a concentration of 60  $\mu\text{l}$ .



useful against MDR infection at a large scale. Antimicrobial activity was observed by the agar well diffusion method. Strain (SA2  $10^{-3}$ ) from *Aloe barbadensis miller* showed strong antimicrobial activity against *Staphylococcus aureus*, *Klebsiella* sp, *Pseudomonas aeruginosa* & *Escherichia coli*. In previous studies, it was reported that silver ion tolerant strain from soil samples showed a zone of inhibition ranging from 10 mm to 19 mm, while biogenic AgNPs of rhizopheric soil didn't show synergetic antimicrobial activity with bioactive metabolites of *Aloe barbadensis miller*.<sup>41,42</sup> Different combinations of biogenic AgNPs and bioactive metabolites were made to evaluate the maximum antimicrobial potential. Among these synergetic potential of combination (*Linum usitatissimum* L & *Aloe barbadensis miller*), WM+SA2( $10^{-3}$ ) was observed as more biologically active against pathogens exhibiting 13–22 mm zone of inhibition. It was observed that bioactive metabolites isolated from different macerated conditions were less effective against MDR infection while showing strong potential in synergetic combination with biogenic AgNPs. Thus, biogenic AgNPs significantly enhance the antimicrobial properties of secondary metabolites.

## 5. Conclusion

In this research, it is concluded that nanotechnology and ethnobotany are potential fields of science due to their potent application in medicine and industry and are environment friendly. Aloe vera was used in the current research to synthesize biogenic silver nanoparticles and shows a safe, accessible, and non-hazardous approach to enhance the potential of bioactive metabolites. This novel research focuses on using bioactive metabolites and biogenic silver nanoparticles against MDR infections instead of using other metal nanoparticles that require laborious methods to isolate. Additionally, the combinations of metabolites and silver nanoparticles show maximum anti-microbial, and antioxidant potential against clinically isolated *Staphylococcus aureus*, *Klebsiella* sp, *Pseudomonas aeruginosa*, and *Escherichia coli* strains. Together, these combinations proved to be effective antimicrobial agents with forthcoming industrial and biomedical applications.

## Data availability

Further data for this research article can be provided as complementary information.

## Conflicts of interest

Authors have no potential conflict of interest.

## Acknowledgements

We are cordially thankful to The Women University Multan and the Higher Education Commission (HEC) Pakistan for their support of this project.

## References

- 1 M. Z. El-Readi, A. M. Al-Abd, M. A. Althubiti, R. A. Almaimani, H. S. Al-Amoodi, M. L. Ashour, M. Wink and S. Y. Eid, *Front. Pharmacol.*, 2021, **12**, 658513.
- 2 A. M. Salih, F. Al-Qurainy, S. Khan, M. Nadeem, M. Tarroum and H. O. Shaikhaldein, *Front. Plant Sci.*, 2022, **13**, 962112.
- 3 H. Chandra, P. Kumari, E. Bontempi and S. Yadav, *Biocatal. Agric. Biotechnol.*, 2020, **24**, 101518.
- 4 S. Kauser, A. Hussain, S. Ashraf, G. Fatima, Ambreen, S. Javaria, Z. U. Abideen, K. Kabir, S. Yaqub, S. Akram, A. Shehzad and S. A. Korma, *Food Chem. Adv.*, 2024, **4**, 100573.
- 5 D. D. Umashankar, *J. Phytopharm.*, 2020, **9**, 270–273.
- 6 S. Noreen, T. Tufail, H. B. Ul Ain and C. G. Awuchi, *Food Sci. Nutr.*, 2023, **11**, 6820–6829.
- 7 S. Anjum, B. H. Abbasi and C. Hano, *Plant Cell, Tissue Organ Cult.*, 2017, **129**, 73–87.
- 8 S. Yousaf, M. Ilyas, A. K. Khattak, S. Z. Satti and I. Jan, *Soil Environ.*, 2017, **36**, 45–50.
- 9 A. M. L. Seca and D. C. G. A. Pinto, *Medicines*, 2019, **6**, 66.
- 10 N. S. Al-Radadi, *Saudi J. Biol. Sci.*, 2022, **29**, 3848–3870.
- 11 R. O. Guerra, J. R. Do Carmo Neto, P. E. F. Da Silva, Y. L. L. Borges, P. I. R. Franco, J. R. Machado and M. V. Da Silva, *Fitoterapia*, 2023, **166**, 105467.
- 12 A. A. Ebrahim, S. S. Elnesr, M. A. A. Abdel-Mageed and M. M. M. Aly, *World's Poult. Sci. J.*, 2020, **76**, 803–814.
- 13 S. Hakim, T. Naqqash, M. S. Nawaz, I. Larai, M. J. Siddique, R. Zia, M. S. Mirza and A. Imran, *Front. Sustain. Food Syst.*, 2021, **5**, 617157.
- 14 M. Tariq, K. N. Mohammad, B. Ahmed, M. A. Siddiqui and J. Lee, *Molecules*, 2022, **27**, 4754.
- 15 T. Mustapha, N. Misni, N. R. Ithnin, A. M. Daskum and N. Z. Unyah, *Int. J. Environ. Res. Public Health*, 2022, **19**, 674.
- 16 A.-C. Burduşel, O. Gherasim, A. M. Grumezescu, L. Mogoantă, A. Ficai and E. Andronescu, *Nanomaterials*, 2018, **8**, 681.
- 17 Y.-W. Zhang, L.-K. Wang, L. Fang-Zhou, B.-H. Yuan, X.-M. Zou and R.-T. Wang, *Inorg. Chem. Commun.*, 2022, **143**, 109781.
- 18 M. M. Ghatage, P. A. Mane, R. P. Gambhir, V. S. Parkhe, P. A. Kamble, C. D. Lokhande and A. P. Tiwari, *Appl. Surf. Sci. Adv.*, 2023, **16**, 100426.
- 19 R. Vishwanath and B. Negi, *Curr. Res. Green Sustainable Chem.*, 2021, **4**, 100205.
- 20 C. F. Silva, L. C. Vitorino, M. A. C. Mendonça, W. L. Araújo, M. N. Dourado, L. C. Albuquerque, M. A. Soares and E. L. Souchie, *S. Afr. J. Bot.*, 2020, **134**, 3–16.
- 21 B. Javed, M. Ikram, F. Farooq, T. Sultana, Z.-R. Mashwani and N. I. Raja, *Appl. Microbiol. Biotechnol.*, 2021, **105**, 2261–2275.
- 22 N. Bharadwaj and N. Siddiqui, *Orient. J. Chem.*, 2021, **37**, 746–751.
- 23 R. Esmail, A. Afshar, M. Morteza, A. Abolfazl and E. Akhondi, *BMC Microbiol.*, 2022, **22**, 97.



- 24 R. Martínez-López and M. G. Tuohy, *Food Chem.:Mol. Sci.*, 2023, **6**, 100166.
- 25 E. Ibrahim, H. Fouad, M. Zhang, Y. Zhang, W. Qiu, C. Yan, B. Li, J. Mo and J. Chen, *RSC Adv.*, 2019, **9**, 29293–29299.
- 26 G. Kahlmeter, C. G. Giske, T. J. Kirn and S. E. Sharp, *J. Clin. Microbiol.*, 2019, **57**, 011299–19.
- 27 K. Logaranjan, A. J. Raiza, S. C. B. Gopinath, Y. Chen and K. Pandian, *Nanoscale Res. Lett.*, 2016, **11**, 520.
- 28 S. O. Aisida, K. Ugwu, P. A. Akpa, A. C. Nwanya, P. M. Ejikeme, S. Botha, I. Ahmad, M. Maaza and F. I. Ezema, *Mater. Chem. Phys.*, 2019, **237**, 121859.
- 29 S. Palithya, S. A. Gaddam, V. S. Kotakadi, J. Penchalaneni and V. N. Challagundla, *Green Chem. Lett. Rev.*, 2021, **14**, 137–152.
- 30 N. Saha, P. Trivedi and S. Dutta Gupta, *J. Cluster Sci.*, 2016, **27**, 1893–1912.
- 31 A. K. Giri, B. Jena, B. Biswal, A. K. Pradhan, M. Arakha, S. Acharya and L. Acharya, *Sci. Rep.*, 2022, **12**, 8383.
- 32 S. Saeed, A. Iqbal and M. A. Ashraf, *Environ. Sci. Pollut. Res.*, 2020, **27**, 37347–37356.
- 33 S. H. Salmen and S. A. Alharbi, *Green Chem. Lett. Rev.*, 2020, **13**, 1–5.
- 34 M. S. Alwhibi, D. A. Soliman, M. A. Awad, A. B. Alangery, H. Al Dehaish and Y. A. Alwasel, *Green Process. Synth.*, 2021, **10**, 412–420.
- 35 S. Sudhimon, M. Mukesh Kumar, S. Yamini, T. Anjana Devi, S. Sumathi and J. Sudagar, *J. King Saud Univ., Sci.*, 2024, **36**, 103317.
- 36 M. S. Alwhibi, D. A. Soliman, M. A. Awad, A. B. Alangery, H. Al Dehaish and Y. A. Alwasel, *Green Process. Synth.*, 2021, **10**, 412–420.
- 37 P. Tippayawat, N. Phromviyo, P. Boueroy and A. Chompoosor, *PeerJ*, 2016, **4**, e2589.
- 38 H. Arshad, M. Saleem, U. Pasha and S. Sadaf, *Electron. J. Biotechnol.*, 2022, **55**, 55–64.
- 39 I.-M. Chung, K. Rekha, G. Rajakumar and M. Thiruvengadam, *3 Biotech*, 2018, **8**, 412.
- 40 M. Hussain, N. I. Raja, Z. Mashwani, F. Naz, M. Iqbal and S. Aslam, *IET Nanobiotechnol.*, 2018, **12**, 514–519.
- 41 N. H. Rezazadeh, F. Buazar and S. Matroodi, *Sci. Rep.*, 2020, **10**, 19615.
- 42 M. A. Huq and S. Akter, *Materials*, 2021, **14**, 2615.

